Potential dual molecular interaction of the *Drosophila* 7-pass transmembrane cadherin Flamingo in dendritic morphogenesis

Hiroshi Kimura[1], Tadao Usui[2], Asako Tsubouchi[2,3] and Tadashi Uemura[2,3,*]

[1]Department of Biophysics, Graduate School of Science, Oiwake-cho, Kitashirakawa, Sakyo-ku, Kyoto 606-8507, Japan
[2]Graduate School of Biostudies, Oiwake-cho, Kitashirakawa, Sakyo-ku, Kyoto 606-8507, Japan
[3]Core Research for Evolutional Science and Technology (CREST), Japan Science and Technology Agency, Kawaguchi, Saitama, 332-0012, Japan
*Author for correspondence (e-mail: tauemura@lif.kyoto-u.ac.jp)

Accepted 8 December 2005
Journal of Cell Science 119, 1118-1129 Published by The Company of Biologists 2006
doi:10.1242/jcs.02832

Summary

Seven-pass transmembrane cadherins (7-TM cadherins) play pleiotropic roles in epithelial planar cell polarity, shaping dendritic arbors and in axonal outgrowth. In contrast to their role in planar polarity, how 7-TM cadherins control dendritic and axonal outgrowth at the molecular level is largely unknown. Therefore, we performed extensive structure-function analysis of the *Drosophila* 7-TM cadherin Flamingo (Fmi) and investigated the activities of individual mutant forms mostly in dendritogenesis of dendritic arborization (da) neurons. One of the *fmi*-mutant phenotypes was overgrowth of branches in the early stage of dendrite development. In da neurons but not in their adjacent non-neuronal cells, expression of a truncated form (ΔN) that lacks the entire cadherin repeat sequence, rescues flies – at least partially – from this phenotype. Another phenotype is observed at a later stage, when dendritic terminals outgrowing from the contralateral sides meet and then avoid each other. In the *fmi* mutant, by contrast, those branches overlapped. Overexpression of the ΔN form on the wild-type background phenocopied the overlap phenotype in the mutant, and analysis in heterologous systems supported the possibility that this effect might be because the Fmi-Fmi homophilic interaction is inhibited by ΔN. We propose that a dual molecular function of Fmi play pivotal roles in dendrite morphogenesis. In the initial growing phase, Fmi might function as a receptor for a so-far-unidentified ligand and this hypothetical heterophilic interaction would be responsible for limiting branch elongation. At a later stage, homophilic Fmi-binding at dendro-dendritic interfaces would elicit avoidance between dendritic terminals.

Supplementary material available online at
http://jcs.biologists.org/cgi/content/full/119/6/1118/DC1

Key words: Cadherin superfamily, Flamingo, Dendrite, *Drosophila*

Introduction

Seven-pass transmembrane cadherins constitute an evolutionally conserved subfamily of the cadherin superfamily (Usui et al., 1999; Tepass et al., 2000; Yagi and Takeichi, 2000; Hirano et al., 2003). In contrast to the studies indicating that classic cadherin is primarily responsible for intercellular adhesion, genetic studies of the *Drosophila* 7-pass transmembrane cadherin Flamingo [Fmi; also known as Starry night (Stan)] have shown its pleiotropic role in intercellular communications by controlling epithelial and neuronal cell morphogenesis (Usui et al., 1999; Chae et al., 1999).

In epithelia, Fmi regulates planar cell polarity (PCP) as a component of one of the non-canonical Frizzled signaling pathways or the PCP pathway (Usui et al., 1999; Chae et al., 1999; Adler, 2002; Mlodzik, 2002; Eaton, 2003; Strutt, 2003; Uemura and Shimada, 2003; Veeman et al., 2003). At least one aspect of its role is the anchoring of signaling molecules that belong to this pathway at adherens junctions, probably occuring through Fmi-Fmi homophilic binding. In neural development of *Drosophila*, Fmi is required for controlling the extension and/or guidance of dendrites and axons of multiple types of neurons (Gao et al., 1999; Gao et al., 2000; Grueber et al., 2002; Lee et al., 2003; Reuter et al., 2003; Senti et al., 2003; Sweeney et al., 2002; Ye and Jan, 2005). Three mammalian homologs of *fmi* (*Celsr1*, *Celsr 2* and *Celsr3*) are differentially expressed in various tissues in the mouse (Formstone and Little, 2001; Shima et al., 2002; Tissir et al., 2002). Crucial roles of 7-pass transmembrane cadherins in PCP, shaping dendritic arbors and axonal tract development, appear to be conserved in mammalian cells (Curtin et al., 2003; Shima et al., 2004; Tissir et al., 2005; Formstone and Mason, 2005).

Whereas Fmi operates in the PCP pathway in epithelia, Fmi-mediated control of dendritic and axonal outgrowth appears to occur separately from the PCP pathway (Gao et al., 2000; Lee et al., 2003; Senti et al., 2003), and the molecular function of Fmi in neurons is largely unknown. In an approach to understand the molecular mechanism, we focused on evolutionally conserved, but complicated, structural features in the family of 7-pass transmembrane cadherins (hereafter referred to as the Flamingo family), and performed extensive in vivo structure-function analysis in *Drosophila*. Extracellular

Journal of Cell Science

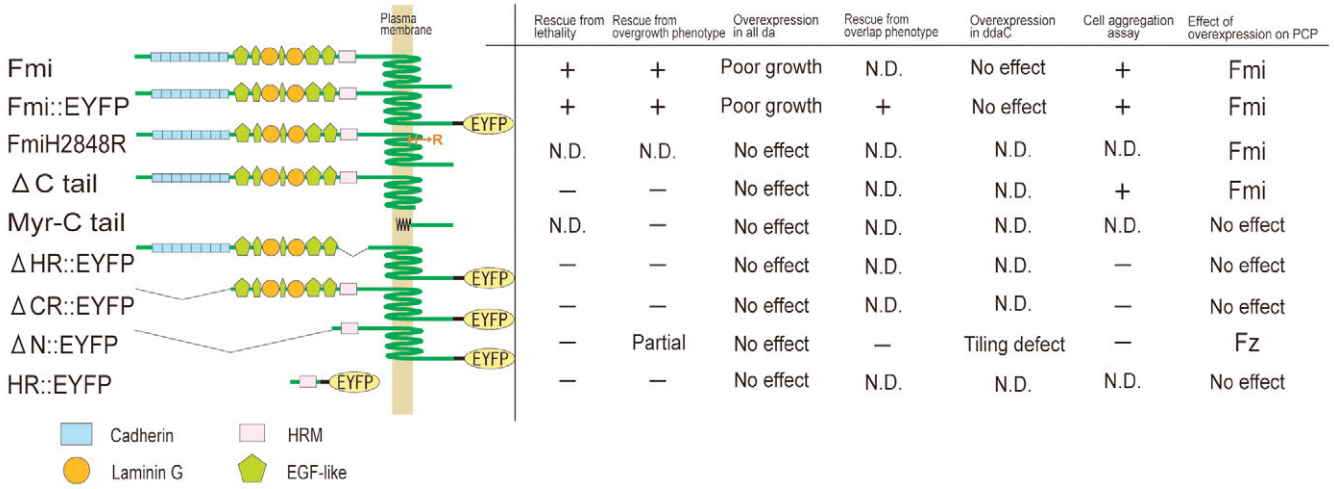

	Rescue from lethality	Rescue from overgrowth phenotype	Overexpression in all da	Rescue from overlap phenotype	Overexpression in ddaC	Cell aggregation assay	Effect of overexpression on PCP
Fmi	+	+	Poor growth	N.D.	No effect	+	Fmi
Fmi::EYFP	+	+	Poor growth	+	No effect	+	Fmi
FmiH2848R	N.D.	N.D.	No effect	N.D.	N.D.	N.D.	Fmi
ΔC tail	–	–	No effect	N.D.	N.D.	+	Fmi
Myr-C tail	N.D.	–	No effect	N.D.	N.D.	N.D.	No effect
ΔHR::EYFP	–	–	No effect	N.D.	N.D.	–	No effect
ΔCR::EYFP	–	–	No effect	N.D.	N.D.	–	No effect
ΔN::EYFP	–	Partial	No effect	–	Tiling defect	–	Fz
HR::EYFP	–	–	No effect	N.D.	N.D.	N.D.	No effect

Fig. 1. Activities of mutant forms of Fmi under various developmental contexts. (Left) Schematic representation of the Fmi protein (3575 aa long) and various mutant forms designed by us. The extracellular region includes eight tandemly repeated cadherin repeats (Cadherin), five EGF-like domains (EGF-like), two laminin G domains (Laminin G), and a hormone receptor domain (HRM). (Right) Results corresponding to the mutant forms shown on the left. 'Rescue from lethality' indicates whether the lethality of *fmi*-null mutants was prevented by expression of either form by using the pan-neuronal driver Gal4-1407 or not. Relevant genotypes were fmi^{E45} *Gal4-1407*/fmi^{E59}; *UAS-transgene*/+. Relevant genotypes of 'rescue from overgrowth phenotype', 'overexpression in all da', 'rescue of overlap phenotype' and 'overexpression in ddaC' were as described in the legends of Figs 2, 3, 4, 5, 6, respectively. Data from the 'cell aggregation assay' are shown in Fig. 8. 'Effect of overexpression on PCP' indicates effects of overexpression on reorientation of wing hairs, as shown in Fig. 9A-D. +, rescue or formation of cell aggregates; – rescue did not occur or cells did not aggregate. Fmi and Fz, effect of overexpression of individual forms resembling that of Fmi and Fz overexpression, respectively (see details in Fig. 9A-D). N.D., not determined. Inactivity of ΔHR::EYFP and ΔCR:EYFP was reminiscent of results of in vivo structure-function analysis of *D*E-cadehrin (Oda and Tsukita, 1999), and we discussed this result and other constructs in Materials and Methods.

regions of the Flamingo family consist of cadherin repeats, which function as homophilic binding modules, and other motifs that are also suggestive of protein-protein interaction (Fig. 1). The sequences of these transmembrane domains show similarity to those of the secretin-receptor family of G-protein-coupled receptors (GPCRs). We made a series of transgenic strains to express various mutant forms of Fmi and addressed how the expression of individual forms affects dendrite morphogenesis and PCP.

We studied the role of Fmi in dendritic morphogenesis in a subset of sensory neurons, i.e. the dendritic arborization (da) neurons (Bodmer and Jan, 1987; Jan and Jan, 1993; Campos-Ortega and Hartenstein, 1997). Growth and elaboration of dendritic arbors of da neurons are easily imaged by whole-mount time-lapse recordings with the help of various green fluorescent protein (GFP) markers (Gao et al., 1999; Grueber et al., 2003; Sugimura et al., 2003). At late embryonic stages, da neurons start growing two-dimensional dendrites underneath the epidermis, and the growth pauses at the end of embryogenesis (explained later; see Fig. 2A, Fig. 3A). Dendritic growth restarts in larvae, and branches keep growing by expanding the body wall in a coordinated fashion. Dendritic terminals of a subclass of da neurons meet mid-way between homologous cells in ispilateral or contralateral adjacent hemi-segments at early larval stages [approximately 30-35 hours after egg laying (AEL)], and tend to turn away before crossing each other (see Fig. 5A, Fig. 6A). This phenomenon is called hetero-neuronal avoidance or tiling, and is mediated by inhibitory interaction at individual dendro-dendritic interfaces (Grueber et al., 2002; Grueber et al., 2003; Sugimura et al., 2003; Jan and Jan, 2003).

Dendrites of dorsal da neurons in *fmi* mutants show two types of phenotype (Gao et al., 2000; Sweeney et al., 2002). In the first, dorsal branches emerge precociously and overextend towards the dorsal midline in the embryos (the 'overgrowth phenotype'; Fig. 2C,E and Fig. 3B). In the second, along the dorsal midline at a later larval stage, dendritic terminals that outgrow from the contralateral sides do not avoid each other, but overlap (the 'overlap phenotype'; Fig. 5B). Although previous mosaic analysis suggests a cell-autonomous role of Fmi in da neurons, we sought to address the question further how Fmi restricts dendritic growth in the embryos and to control heteroneuronal avoidance in the larvae. On the basis of previous studies and our structure-function analysis, we discuss the possibility that Fmi controls the early outgrowth and the mutual avoidance by way of two distinct mechanisms.

Results

Quantification of rescue of the dendritic overgrowth phenotype by neuron-specific Gal4 strains

Branches in the dorsal region of *fmi*-mutant embryos overextended towards the dorsal midline and, in addition, lateral branches either showed poor growth or were misrouted dorsally (Fig. 2C) (Gao et al., 1999; Gao et al., 2000). Flies were rescued from the overshooting phenotype by expressing the *fmi* transgene in the entire nervous system or in all da neurons (Gao et al., 2000). By using our Gal4 drivers that label a small subset of da neurons (Sugimura et al., 2003; Sugimura et al., 2004), we visualized phenotypes with higher resolution and quantitatively assessed the rescue activity of individual Fmi forms. One of those drivers, IH1 GAL4, highlighted two

Journal of Cell Science

Journal of Cell Science

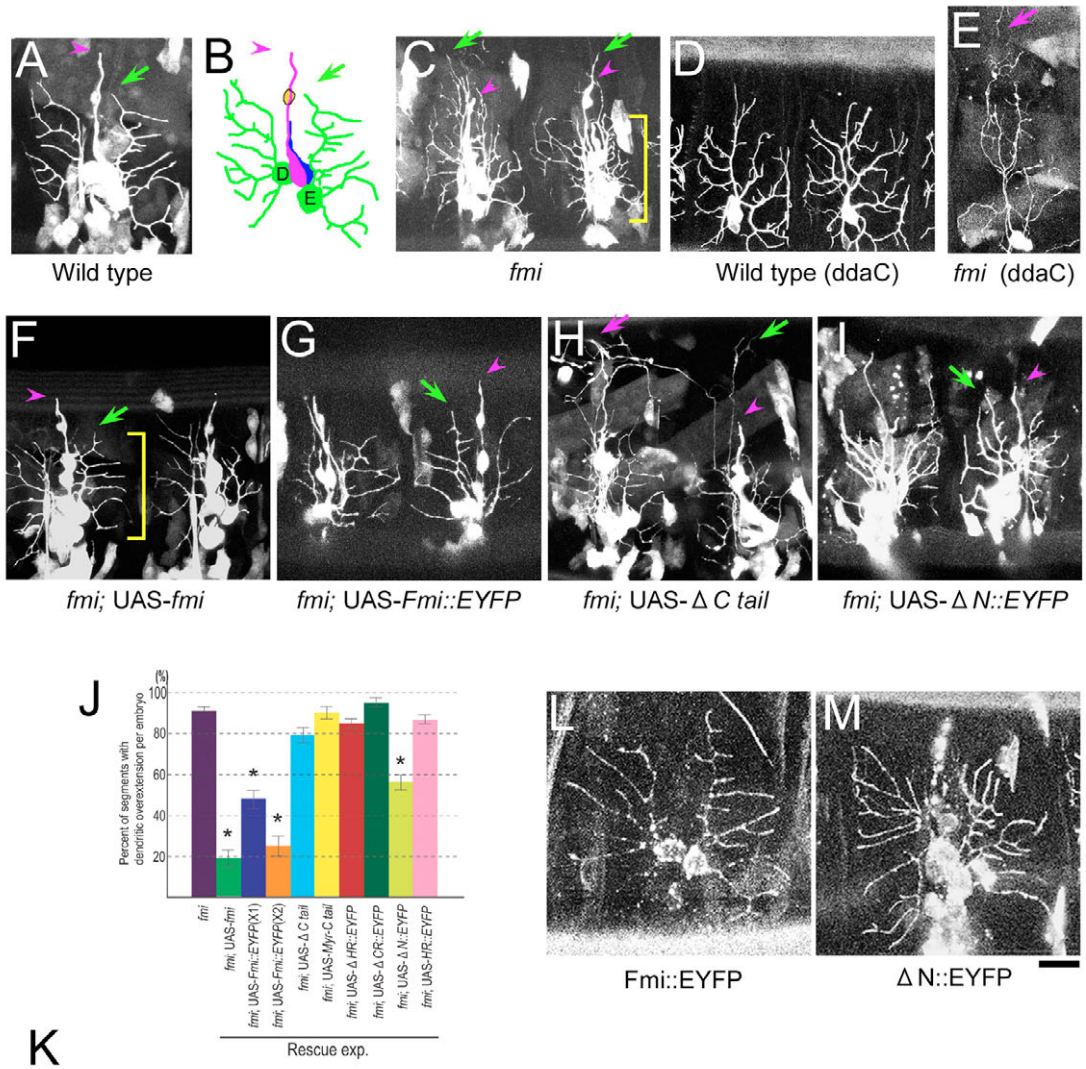

K

Abbreviations in A,C,and F-J	Genotypes	Number of segments with dendritic overextension / Number of total segments	(%)	Number of embryos
Wild type	IH1-GAL4, UAS-GFP / IH1-GAL4, UAS-GFP	0/ 32	(0%)	4
fmi	IH1-GAL4, UAS-GFP, fmi^{E59} / IH1-GAL4, UAS-GFP, fmi^{E59}	112/122	(91%)	15
fmi; UAS-*fmi*	IH1-GAL4, UAS-GFP, fmi^{E59} / IH1-GAL4, UAS-GFP, fmi^{E59} : UAS-fmi / UAS-fmi	20/106	(19%)	14
fmi; UAS-*Fmi::EYFP*(X1)	IH1-GAL4, UAS-GFP, fmi^{E59} / IH1-GAL4, UAS-GFP, fmi^{E59} : UAS-fmi::EYFP / +	58/122	(48%)	15
fmi; UAS-*Fmi::EYFP*(X2)	IH1-GAL4, UAS-GFP, fmi^{E59} / IH1-GAL4, UAS-GFP, fmi^{E59} : UAS-fmi::EYFP / UAS-fmi::EYFP	33/134	(25%)	17
fmi; UAS-Δ *C tail*	IH1-GAL4, UAS-GFP, fmi^{E59} / IH1-GAL4, UAS-GFP, fmi^{E59} : UAS-Δ Ctail / UAS-Δ Ctail	107/136	(79%)	17
fmi; UAS-*Myr-C tail*	IH1-GAL4, UAS-GFP, fmi^{E59} / IH1-GAL4, UAS-GFP, fmi^{E59} : UAS-myrCtail / UAS-myrCtail	102/ 112	(90%)	14
fmi; UAS-Δ *HR::EYFP*	IH1-GAL4, UAS-GFP, fmi^{E59} / IH1-GAL4, UAS-GFP, fmi^{E59} : UAS-Δ HR::EYFP / UAS-Δ HR::EYFP	100/ 118	(85%)	14
fmi; UAS-Δ *CR::EYFP*	IH1-GAL4, UAS-GFP, fmi^{E59} / IH1-GAL4, UAS-GFP, fmi^{E59} : UAS-Δ CR::EYFP / UAS-Δ CR::EYFP	106/ 112	(95%)	14
fmi; UAS-Δ *N::EYFP*	IH1-GAL4, UAS-GFP, fmi^{E59} / IH1-GAL4, UAS-GFP, fmi^{E59} : UAS-Δ N::EYFP / UAS-Δ N::EYFP	70/123	(57%)	14
fmi; UAS-*HR::EYFP*	IH1-GAL4, UAS-GFP, fmi^{E59} / IH1-GAL4, UAS-GFP, fmi^{E59} : UAS-HR::EYFP / UAS-HR::EYFP	98/ 113	(87%)	14

Fig. 2. Rescue of *fmi* mutant embryos from the dendritic overgrowth phenotype by mutant forms of Fmi. (A-I) Visualization by use of GFP of a subset of da neurons in the abdominal dorsal cluster in embryos at 20-22 hours AEL. In these and all subsequent panels of embryos and larvae, dorsal is at the top and anterior is to the left unless described otherwise. (A-C,F-I,L,M) Class I da neurons (ddaD and ddaE) and es neurons are labeled in the (A) wild type, (C) fmi^{E59}/fmi^{E59} mutant and (F) a mutant expressing a transgene of either *fmi*, *fmi::EYFP* (G), *ΔC* (H), or *ΔN::EYFP* (I). Arrows indicate terminals of two da neurons, ddaD and ddaE [green cells in (B) tracing]; arrowheads indicate terminals of es neurons [magenta cell in (B) tracing]. In the tracing, one of the es neuron accessory cells (yellow) is also drawn. In contrast to the wild type (A,B), the *fmi* mutant extended the da dendrites more dorsally than es dendrites (C). Yellow bracket in C indicates lateral branches that showed undergrowth and/or misrouting. Neuronal expression of (F) Fmi and (G) Fmi::EYFP but not that of (H) ΔCtail, prevented both the dorsal overgrowth and malformation of lateral branches (bracket in F), whereas the rescue effect of ΔN::EYFP was partial (I,J). Overextended dendrites of the contralateral counterpart are indicated by a magenta arrow (H). Detailed genotypes of individual panels are described in K. The Gal4 driver used in this rescue experiment was IH1. Although IH1-driven Fmi expression prevented the phenotype, it did not cure embryonic lethality of the fmi^{E59}/fmi^{E59} mutant, probably because IH1 drove transgene expression only in a small subset of neurons of the CNS and PNS. (D,E) Dendritic morphology of a class IV ddaC in the (D) wild type or in (E) the *fmi* mutant. ddaC dendrites in the mutant overextended dorsally and a contralateral branch terminal is indicated by an arrow in E. Genotypes were (D) *NP1015 Venus-pm* and (E) *NP7028 GFP[S65T]* $fmi^{E59}/$*NP7028 GFP[S65T]* fmi^{E59}. (J,K) Quantitative analysis of the rescue experiments. Bars represent percentages of hemi-segments that showed the overgrowth in embryos of individual genotypes. Each of the full-length or mutant forms of Fmi was produced from two copies of each transgene in the mutant, except *fmi*; *UAS-Fmi::EYFP (X1)*. *, statistically significant rescue (P<0.005), compared with the phenotypic penetrance of the mutant (Student's t-test). Table K summarizes genotypes and quantification. (L,M) Subcellular localizations of (L) Fmi::EYFP and (M) ΔN::EYFP. Image of EYFP fluorescence of (L) *IH1-GAL4/IH1-GAL4*; *UAS-fmi::EYFP/UAS-fmi::EYFP* and of (M) *IH1-GAL4/IH1-GAL4*; *ΔN::EYFP/ΔN::EYFP*. Bar in M: 14.5 μm for A, 20 μm for C-I, 10 μm for L,M.

Journal of Cell Science

dorsal da neurons (ddaD and ddaE) as well as external sensory (es) neurons in the embryo (Fig. 2A,B).

To judge the dendritic overgrowth of ddaD and ddaE, we took advantage of the relative position of dendritic tips of the ddaD and ddaE neurons and the es neurons in the embryos just before hatching (20-22 hours AEL). In the wild type, tips of the es neurons were located more dorsally than those of ddaD and ddaE neurons (in 32 out of 32 abdominal hemi-segments examined; A2-A6) (Fig. 2A,B arrows and arrowheads). By contrast, dendrites of ddaD and ddaE neurons extended more dorsally than those of es neurons in 91% of the hemi-segments of *fmi* null mutant embryos (Fig. 2C). This high penetrance was reduced to 19% when two copies of the *fmi* transgene were expressed in the mutant (Fig. 2F,J,K). We also expressed in the mutant the full-length Fmi, which had been tagged with enhanced yellow fluorescent protein (EYFP) (Fmi::EYFP), and showed that two copies of Fmi::EYFP exhibited a rescue activity with respect to both the overgrowth phenotype and lethality that was similar to the presence of two copies of the untagged Fmi transgene (Fig. 2G,J,K). Not only the dorsal overgrowth phenotype, but also poor growth in lateral directions was prevented by expression of Fmi or Fmi::EYFP (see brackets in Fig. 2C,F). It should be noticed that neither the distance between cell bodies of es neurons and da neurons nor the length of the es dendrite was significantly altered in wild-type, mutant and rescued animals (data not shown). The overgrowth phenotype is not specific to ddaD and ddaE neurons, shown by the fact that dendrites of a third da neuron, ddaC, also displayed dorsal overextension (Fig. 2, compare D with E). Since none of the Gal4 lines in this or previous studies appeared to drive transgenic expression in embryonic epidermal cells that might make contact with dendrites, the significant rescue by these drivers suggests that *fmi* is necessary for normal dendritic growth in da neurons but not, as previously discussed, in epidermis (Gao et al., 2000; Ye and Jan, 2004).

ΔN::EYFP, a form without cadherin repeats, partially rescues the mutant embryos from the overgrowth phenotype

Individual forms of the designed Fmi-mutants (illustrated in Fig. 1) were examined to see whether their expression can prevent the overgrowth phenotype and whether their overexpression can exert a dominant phenotype on the wild-type background. Among the deletions and truncations examined, ΔN::EYFP gave the most interesting results that are described below. Although ΔN::EYFP lacks almost all of the conserved extracellular motifs except for a hormone-receptor domain (HRM), its expression in da neurons partially rescued the mutant embryos from the overgrowth phenotype (Fig. 2I,J). The HRM is about 60 amino acids (aa) long and conserved in the subfamily of G-protein coupled receptors (GPCRs) (supplementary material Fig. S1); conserved cysteine residues in HRM have been implicated in transmitting signals of ligand binding to intracellular components (Asmann et al., 2000). We collected images of da neurons in live animals that expressed either Fmi::EYFP or ΔN::EYFP, quantified EYFP fluorescence of the neurons expressing either form, and showed that the expression level of ΔN::EYFP was comparable to that of Fmi::EYFP (supplementary material Fig. S2).

The rescue effect of ΔN::EYFP expression on the overgrowth phenotype was also investigated in a different way of quantification, in which the distance between tips of dendritic terminals and the dorsal midline was measured in embryos 21-22 hours AEL (Fig. 3). In the wild-type embryo, dendritic terminals do not reach the dorsal midline, leaving dendrite-free zones on both sides of the dorsal midline (Fig. 3A). By contrast, about 80% of the terminals in the mutant reached the midline before hatching (Fig. 3B). The distribution of the distance was compared between the wild type, the *fmi* mutant, and the *fmi* mutants expressing Fmi::EYFP or ΔN::EYFP, and the partial rescue activity of ΔN::EYFP was again indicated (Fig. 3C,D). As predicted from the absence of

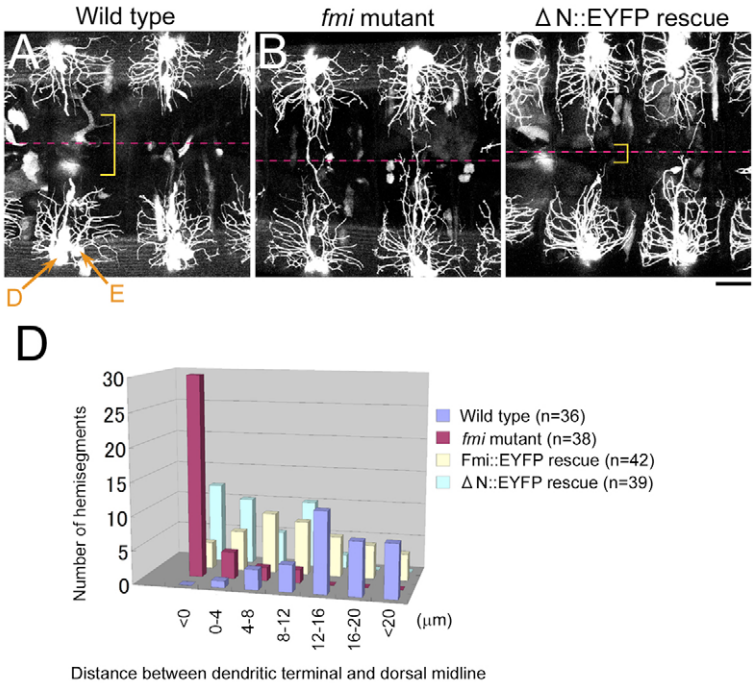

Fig. 3. Experiment showing partial rescue from the overgrowth phenotype by expression of ΔN::EYFP. (A,B) Dorsal front views of embryos of 21-22 hours AEL in which a large subset of da neuron expressed GFP. Broken lines represent dorsal midlines. (A) In the wild-type embryo, dendritic terminals of ddaD and ddaE (D and E) did not reach the dorsal midline, and dendrite-free zones were observed (bracket). (B) In contrast, branch terminals in the *fmi* null mutant reached the midline before hatching. (C) ΔN::EYFP expression partially prevented the dorsal overgrowth (bracket). Bar, 20 μm. (D) Distribution of the distance between the most dorsal tips of dendritic terminals of ddaD and ddaE and the dorsal midline in each hemi-segment. The label <0 on *x*-axis indicates that branch terminals extended beyond the midline and invaded contralateral hemi-segments. Relevant genotypes were *Gal109(2)80 UAS-GFP[S65T]/IH1 UAS-GFP[S65T]* (A, and Wild type in D), *Gal109(2)80 UAS-GFP[S65T] fmi^{72}/IH1 UAS-GFP[S65T] fmi^{E59}* (B, and *fmi* mutant in D), *Gal109(2)80 UAS-GFP[S65T] fmi^{72}/IH1 UAS-GFP[S65T] fmi^{E59}*; *UAS-fmi::EYFP/UAS-fmi::EYFP* (Fmi::EYFP rescue in D), and *Gal109(2)80 GFP[S65T] fmi^{72}/IH1 GFP fmi^{E59}*; *UAS-ΔN::EYFP/UAS-ΔN::EYFP* (C, and ΔN::EYFP rescue in D). Numbers of abdominal segments examined for individual genotypes are indicated.

Journal of Cell Science

cadherin repeats, expression of ΔN::EYFP in S2 cells did not lead to the formation of cell aggregates, whereas expression of Fmi or Fmi::EYFP did (Fig. 8).

In the wild-type embryo, dendrites of da neurons extend on the basal surface of the epidermis, and both da neurons and epidermis express Fmi (Usui et al., 1999; Gao et al., 2000). As described above, expression of *fmi* in mutant da neurons was sufficient to rescue the *fmi*-mutant embryos from the dendritic phenotype (Gao et al., 2000; this study). Under the rescue condition described in Fig. 2, Fmi::EYFP or ΔN::EYFP were distributed in dendrites and cell bodies in a splotchy fashion (Fig. 2L,M), reminiscent of the distribution of endogenous Fmi molecules in the wild-type neurons. However, obvious signals of Fmi::EYFP or ΔN::EYFP were not detected in the overlying epidermis. Together with our data of the partial rescue by ΔN::EYFP, all these results are difficult to explain by the hypothesis that the homophilic Fmi-Fmi interaction between dendrites and epidermis plays a crucial role in controlling dendritic extension. One possible explanation of the rescue is that Fmi interacts in a heterophilic manner with an unknown molecule that restricts dendritic growth. The extracellular region of ΔN::EYFP, which consists of a HRM and a segment more proximal to the membrane, together with extracellular loops of the 7-pass transmembrane domain, might be involved in such a hypothetical heterophilic interaction (Fig. 10A). Alternatively, the role of Fmi in dendritic growth restriction might not require any extracellular signals.

Overexpression of Fmi or Fmi::EYFP results in undergrowth of dendrites

To pursue whether overexpression of any forms of Fmi on the wild-type background exerts a dominant effect on dendritic growth, we explored phenotypes when robustly expressing individual Fmi mutant forms in da neurons, by using a total of four copies of two postmitotic, pan-da Gal4 insertions, *109(2)80* and *IG1-2* (Fig. 4).

Overexpression of Fmi or Fmi::EYFP gave rise to strong and highly penetrant phenotypes. In all of the observed 40 dorsal clusters, both the total length of dendrites and the number of terminals greatly decreased, although the number of cells per cluster did not change (Fig. 4, compare A with B). However, no other form, including ΔN::EYFP, affected dendrite formation (Fig. 4C). These results strengthen the proposed role of Fmi in limiting dendritic growth. Moreover, they support the idea that Fmi::EYFP is functionally equivalent to Fmi and that the activity of ΔN::EYFP to restrict growth is substantially weaker than that of the full-length molecules. It has previously been reported that Fmi overexpression [by using two copies of *109(2)80*] caused a dendritic overgrowth that is similar to the mutant phenotype, although overexpression-induced overextension was much less penetrant than the phenotype seen in the mutant (10%) (see Gao et al., 2000). Because both the previous and our study used the same UAS transgenic strain (Usui et al., 1999), the difference in results appeared to be due to distinct levels of overexpression, because of different copy numbers of *Gal4* drivers and/or protocols to assess dendritic overgrowth.

Fmi::EYFP prevents the dorsal-dendrite-overlap phenotype at larval stages, whereas ΔN::EYFP does not

As described above, ΔN::EYFP appeared to retain the partial activity to control dendritic growth in the embryo. Can the same

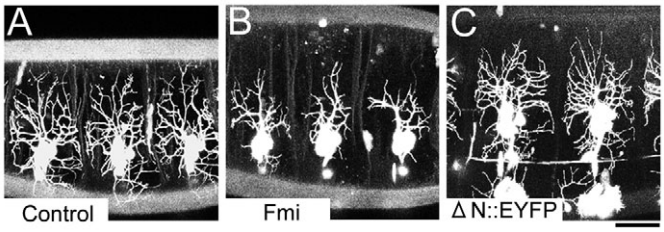

Fig. 4. Overproduction of Fmi in the wild-type background caused underdevelopment of dendrites. (A) Dorsal clusters in a control embryo of 20-22 hours AEL where all da neurons expressed GFP. (B) Overproduction of the wild-type form of Fmi resulted in poor dendritic growth and a decrease in the number of branches. (C) Overproduction of ΔN::EYFP did not cause an obvious morphological defect. Genotypes were *IG1-2 Gal109(2)80 UAS-GFP[S65T]/IG1-2 Gal109(2)80 UAS-GFP[S65T]* (A), *IG1-2 Gal109(2)80 UAS-GFP[S65T]/IG1-2 Gal109(2)80 UAS-GFP[S65T]*; *UAS-fmi/UAS-fmi* (B), and *IG1-2 Gal109(2)80 UAS-GFP[S65T]/IG1-2 Gal109(2)80 UAS-GFP[S65T]*; *UAS-ΔN::EYFP/UAS-ΔN::EYFP* (C). Bar, 30 μm. Embryos that were homozygous for *IG1-2 Gal109(2)80 UAS-GFP[S65T]* did not hatch, so we could not observe how Fmi overexpression in this genotype that had total four copies of *Gal4* affected dendrite morphogenesis at larval stages.

form rescue the mutant animals form the dorsal-dendrite-overlap phenotype at later larval stages? To address this question, we expressed either Fmi::EYFP or ΔN::EYFP in trans-heterozygotes fmi^{72}/fmi^{E59} that survived until early- to mid-larval stages (Fig. 5, details of genotypes are described in the legend). In the trans-heterozygous larvae, terminals of dorsal dendrites that had extended from contralateral sides crossed or overlapped each other in 25 out of 26 abdominal segments examined at 32-35 hours AEL (Fig. 5, compare A with B). To selectively visualize dendritic terminals of class IV da neurons that display significant interneuronal avoidance in normal development (Grueber et al., 2002; Grueber et al., 2003; Sugimura et al., 2003), we ablated da neurons of all the other classes in dorsal clusters of one hemi-segment and its contralateral counterpart, but left one pair of class IV ddaC alone. This experiment showed that terminals of the adjacent ddaC neurons did not avoid each other in five out of five segments examined in the *fmi* mutants (Fig. 5, compare D,G with E,H).

This penetrant overlap phenotype was substantially prevented by Fmi::EYFP expression (Fig. 5C). By contrast, it was hardly cured by ΔN::EYFP expression in any of the six segments, where only class IV dendrites were visualized (Fig. 5F,I), which suggests the inability of ΔN::EYFP to act for heteroneuronal avoidance between dorsal dendrites. These data suggest that extracellular motifs, which were missing in ΔN::EYFP, are necessary for the inhibitory dendro-dendritic interaction.

ΔN::EYFP expression on the wild-type background causes dendritic terminals to cross each other

To investigate the molecular mechanism how Fmi operates in the avoidance between dorsal dendritic terminals, we explored whether expression of ΔN::EYFP (which failed to prevent the overlap phenotype) exerts a dominant-negative effect on the wild-type background or not. To assess the effect of ΔN::EYFP expression at high resolution, we employed the driver NP1161

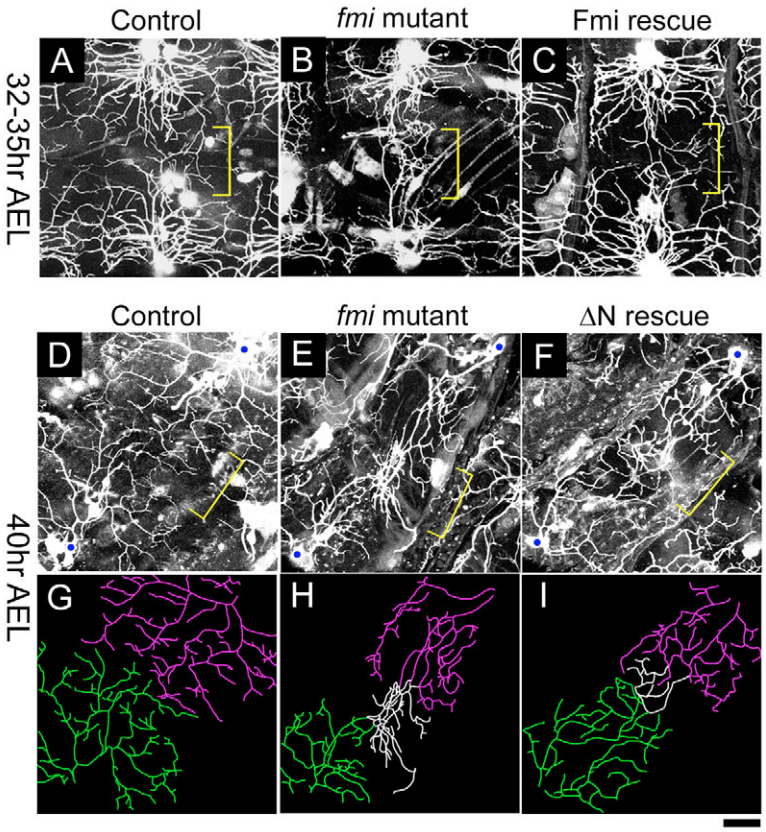

Fig. 5. Fmi::EYFP prevented the dorsal-dendrite-overlap phenotype, whereas ΔN::EYFP did not. (A-C and D-F) Dorsal front views of abdominal segments at 32-35 hours AEL and those at about 40 hours AEL, respectively. (A-C) A large subset of da neurons in dorsal clusters expressed GFP. (D-F) Essentially all da neurons except for ddaC were ablated in dorsal clusters of one hemi-segment and its contralateral counterpart by laser. Blue circles indicate cell bodies of the ddaC. Brackets indicate dendritic terminals that met midway between contralateral da neurons. Anterior is at the top left. (G-I) Tracing of dendritic branches that are shown in the respective panels D-F above. Dendrites that belonged to one of the adjacent hemi-segments are green or magenta, whereas intertwining branches that were difficult to track down are white. (A,D) Control larvae in which dendritic branches covered the whole body walls with minimum overlap. (B and E) In *fmi* mutant larvae, dendritic terminals that had extended from contralateral sides did not turn away, but rather overlapped or crossed with each other (bracket). Fmi::EYFP expression in da neurons in the *fmi* mutants rescued the larvae from the overlap phenotype (C), whereas ΔN::EYFP expression did not confer an inhibitory interaction between terminals (F). Genotypes were *Gal109(2)80 UAS-GFP[S65T]/IH1 UAS-GFP[S65T]* (A and D), *Gal109(2)80 UAS-GFP[S65T] fmi^{72}/IH1 UAS-GFP[S65T] fmi^{E59}* (B and E), and *Gal109(2)80 UAS-GFP[S65T] fmi^{72}/IH1 UAS-GFP[S65T] fmi^{E59}*; *UAS-fmi/UAS-fmi* (C), and *Gal109(2)80 UAS-GFP[S65T] fmi^{72}/IH1 UAS-GFP[S65T]fmi^{E59}*; *UAS-ΔN::EYFP/UAS-ΔN::EYFP* (F). Bars in I: 20 μm for A-C and 17 μm for D-I.

and marker ppk-EGFP for class IV da neurons (including ddaC), which extend dendritic terminals far enough to encounter terminals of counterpart cells in adjacent hemi-segments (Grueber et al., 2003; Sugimura et al., 2003; Sugimura et al., 2004).

In all of the more than 50 dorsal segments examined in the control larvae, sharp boundaries were generated between contralateral dendritic territories (Fig. 6A,A'). By contrast, ΔN::EYFP expression caused incomplete segregation of dendritic terminals in six out of the 50 segments observed (Fig. 6B,B'). ΔN::EYFP-expressing dendritic terminals overlapped with each other along the midline, and it was difficult to judge, to which cell individual terminals belonged (Fig. 6A'-C', white terminals). Furthermore, terminals occasionally invaded the territory of contralateral ddaC (Fig. 6B'and C, arrowheads). The effect of ΔN::EYFP-expression was reproduced by using another Gal4 driver, ppk-Gal4, allowing us to express ΔN::EYFP and membrane-bound GFP in ddaC as well as

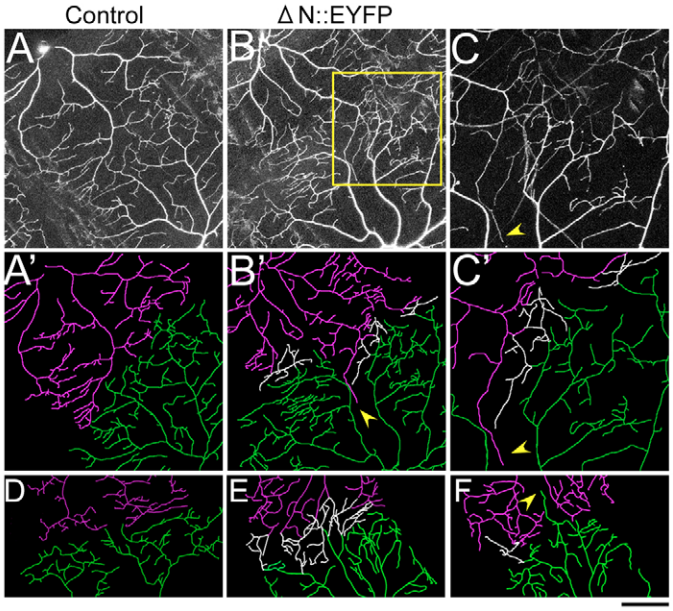

Fig. 6. ΔN::EYFP overexpression on the wild-type background caused dendritic terminals to cross each other. Dorsal views of larvae at about 50 hours AEL in which dendrites of ddaC (class IV) were visualized. Anterior is at the bottom left. (A-C) Dendritic morphology of ddaC in a control larva (A) and a larva that expressed ΔN::EYFP by using *NP1161* in ddaC (B). The boxed area in B is magnified in C. (A'-C') Tracing of dendritic branches that are shown in each of the upper panels. The braches were colored like in Fig. 5G-5I. (D-F) Tracing of dendrites of other ddaC cells visualized by another driver, *ppk-Gal4*. (D) A control larva. (E and F) Larva that expressed ΔN::EYFP. In the control larva, dendrites of ddaC did not cross over with those of contralateral counterparts (A, A' and D). By contrast, dendrites of ΔN::EYFP-expressing ddaC failed to avoid each other and sometimes invaded contralateral hemi-segments (arrowhead in B', C,C',F). Genotypes were *NP1161/NP1161; ppk-EGFP/ppk-EGFP* (A and A'), *NP1161/UAS-ΔN::EYFP; ppk-EGFP/ppk-EGFP* (B,C,B',C'), *ppk-Gal4 UAS-mCD8-GFP/ppk-Gal4 UAS-mCD8-GFP* (D), and *ppk-Gal4 UAS-mCD8-GFP/ppk-Gal4 UAS-mCD8-GFP; UAS-ΔN::EYFP/UAS-ΔN::EYFP* (E and F). Bars in F: 50 μm for A,B,A',B'; 25 μm for C,C'; 60 μm for D-F.

another *UAS-ΔN::EYFP* stock in which the transgene was inserted into a different chromosome (Fig. 6D-F; see legend for details of genotypes). In contrast to those of the control (Fig. 6D), dendritic terminals of ΔN::EYFP-expressing ddaCs overlapped with each other and/or invaded the contralateral hemi-segment in about 20% of the segments examined (Fig. 6E,F). Such overlap and invasion phenotypes were not observed when Fmi::EYFP was expressed on the wild-type background using the same drivers (data not shown). The Fmi::EYFP expression in Fig. 6 did not cause growth restriction, either, probably because the expression levels shown in Fig. 6 were lower than that shown in Fig. 4C (compare genotypes described in both figure legends).

ΔN::EYFP expression decreases the level of endogenous Fmi at intercellular boundaries in epithelial cells

How does ΔN::EYFP overexpression interfere with the inhibitory communication at dendro-dendritic interfaces? ΔN::EYFP might affect the intracellular localization of endogenous Fmi molecules. This hypothesis was technically challenging to verify in dendrites of da neurons, because da dendrites are too thin to examine whether labeled proteins are distributed on the plasma membrane or not. Therefore, we tested our hypothesis by using imaginal epithelia, where Fmi is localized at apically positioned adherens junction and binds in a homophilic manner at intercellular boundaries (Fig. 7) (Usui et al., 1999).

The Fmi level at cell boundaries was dramatically decreased inside the ΔN::EYFP-expression domain (Fig. 7A-F). ΔN::EYFP expression did not lead to disruption of either cell-to-cell adhesion or adherens junction, as shown by the fact that the cell adhesion molecule *D*E-cadherin was still located at the apical intercellular boundaries (data not shown). This result suggests that ΔN::EYFP expression either downregulates the level of Fmi within each cell and/or relocates Fmi from adherens junction to either apical free cell surfaces, basolateral membrane domains or intracellular compartments. By extrapolation, we speculate that endogenous Fmi can hardly be present at dendro-dendritic interfaces when ΔN::EYFP-expressing branch terminals meet.

In contrast to the substantial decrease in the Fmi level between cells with high ΔN::EYFP expression, Fmi accumulated preferentially at those interfaces, where cells with distinct levels of ΔN::EYFP juxtaposed each other (Fig. 7D-I). This was prominent along the borders of the expression domain (Fig. 7D-F, arrowheads) and also within the expression domain that was mosaic in terms of the expression level (Fig. 7G-I, arrowheads). These interface accumulations provided a contrast to what happens along borders of *fmi* mutant clones, namely that Fmi is totally missing at any cell boundaries between *fmi*+ and *fmi*– cells (Usui et al., 1999). Therefore, at least in the ΔN::EYFP-expressing cells that made contact with non- or hardly expressing cells, Fmi molecules were not degraded or prevented to exit the ER or Golgi network but redistributed to those cell contact sites.

Coexpression of ΔN::EYFP with Fmi inhibites Fmi-mediated homophilic cell adhesion

The above results of ΔN::EYFP expression in imaginal discs motivated us to study whether its high-level expression would be able to inhibit Fmi-Fmi homophilic interaction in the cell culture system (Usui et al., 1999) or not. We first studied whether expression of the wild-type or each of the mutants results in the formation of cell aggregates or not (Fig. 8A-8F; see also Materials and Methods). In contrast to Fmi-expressing S2 cells, which formed large aggregates, cells that coexpressed Fmi and ΔN::EYFP did not show such an adhesive property. Moreover, this effect of the coexpression depended on the relative dose of a transfected expression plasmid of Fmi to that of ΔN::EYFP (Fig. 8G,H). Under the condition in which cells coexpressing Fmi and ΔN::EYFP did not form aggregates, our western analysis showed that the level of Fmi was not reduced compared with that in cells expressing Fmi alone (data not shown), favoring the idea that ΔN::EYFP expression does not downregulate the overall level of Fmi.

How does ΔN::EYFP inhibit Fmi-Fmi homophilic interaction at the molecular level?

The structure of ΔN::EYFP and the effects of its expression are reminiscent of those of a dominant-negative form of classic cadherin, which lacks almost all of its extracellular region but retains its transmembrane domain and the catenin-binding intracellular tail (Fujimori and Takeichi, 1993). When this form was expressed in a keratinocyte cell line, endogenous cadherins localizing at cell-cell boundaries was

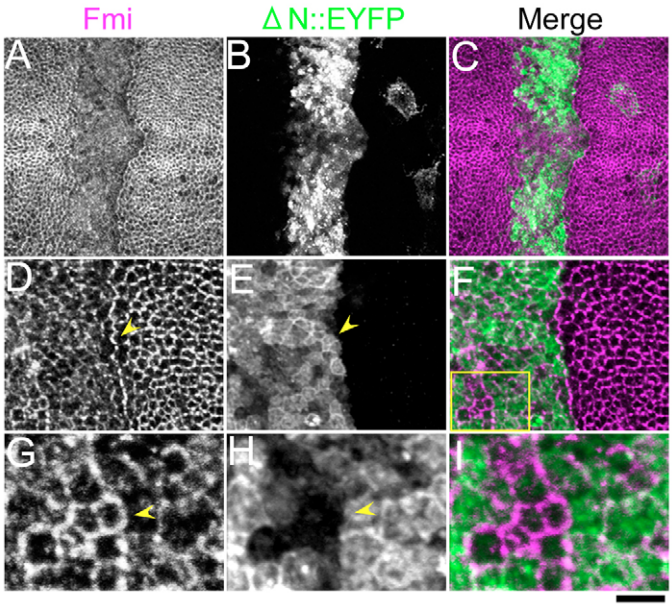

Fig. 7. ΔN::EYFP expression decreased the level of Fmi at intercellular boundaries in wing epithelia. (A-I) ΔN::EYFP was expressed by *ptc-Gal4* in wing imaginal discs of 3rd instar larvae. Anterior is to the left. Imaginal discs were stained for endogenous Fmi (A, D, G; magenta in C,F,I), EYFP (B,E,H; green in C,F,I). (C,F,I) Merged images. (D-F) Higher-magnification images of AP boundaries. (A-F) When adjacent cells strongly expressed ΔN::EYFP, the level of endogenous Fmi was reduced at cell-cell boundaries. (G-I) Boxed area in F shown higher-magnification image in I. Endogenous Fmi was localized at boundaries of cells that expressed ΔN::EYFP at distinct levels (arrowheads in G,H). Bar in I: 11.5 μm for A-C; 5.5 μm for D-F; 2 μm for G-I.

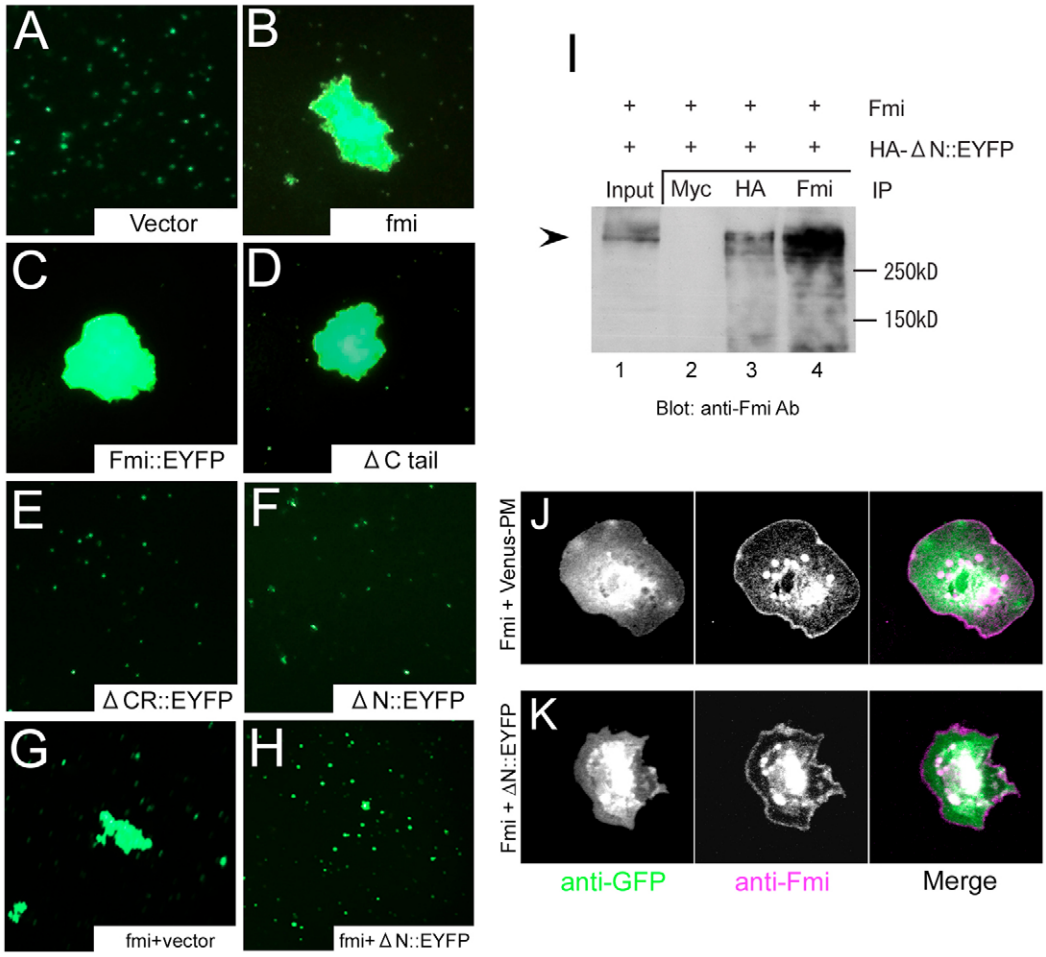

Fig. 8. ΔN::EYFP inhibited Fmi-dependent cell aggregation and might have interacted with Fmi in cultured cells. (A-F) S2 cells were transfected with a plasmid without insert (A) or with one of plasmids encoding various Fmi forms (B-F), together with an EGFP plasmid; and they were examined to see whether they formed aggregates or not. Cells that expressed Fmi (B), Fmi::EYFP (C), or ΔCtail (D) assembled, but those that expressed ΔCR::EYFP (E) or ΔN::EYFP (F) did not. (G,H) Coexpression of ΔN::EYFP with Fmi inhibited Fmi-dependent cell aggregate formation. S2 cells were co-transfected with the EGFP plasmid and the Fmi expression plasmid, together with one without insert (G) or with the ΔN::EYFP plasmid (H). (I) Fmi and HA-ΔN::EYFP were expressed in HEK293T cells. The cell lysate (lane 1) and immunoprecipitates (IP) obtained with either anti-myc (negative control, lane 2), anti-HA (lane 3), or anti-Fmi (lane 4) were blotted with anti-Fmi antibodies. The arrowhead points to Fmi molecules. Fmi was coimmunoprecipitated with HA-ΔN::EYFP (lane 3). (J,K) S2 cells were transfected with a plasmid expressing (J) membrane-bound Venus (Venus-pm) or with (K) ΔN::EYFP plasmid, together with the Fmi expression plasmid. Cells were spread on ConA-coated dishes and stained for GFP (left panels; green in merged right panels) and Fmi (middle panels; magenta in merged right panels). We used 0.05% saponin to permeabilize plasma membranes in order to preserve intracellular vesicular structures. Over 20 cells were observed for each transfection experiment and all cells showed similar protein distributions to cells shown in J and K.

largely diminished, although the amount of E-cadherin was not significantly affected. Classic cadherins have been shown to dimerize in cis or laterally (between molecules on the same cell) as well as in trans (molecules from adjacent cells), and it has been suggested that the lateral dimeric structure is necessary for intercellular adhesive activity (Ozawa, 2002; Patel et al., 2003). It has been proposed that this lateral molecular interaction is inhibited by the dominant-negative form (Fujimori and Takeichi, 1993).

We hypothesized that ΔN::EYFP exerts its effect on Fmi-mediated homophilic interaction in an analogous fashion, and so examined whether ΔN::EYFP physically interacts with Fmi or not (Fig. 8I). Coexpression of Fmi and HA-tagged ΔN::EYFP in HEK293T and subsequent immunoprecipitation showed that Fmi molecules coimmunoprecipitated with ΔN::EYFP. This result implies the possibility that Fmi and ΔN::EYFP interact with each other in the same cells and that this molecular interaction exerts its dominant effect over Fmi-Fmi binding at intercellular contact sites. This binding of ΔN::EYFP to Fmi might either lead to the internalization of the ΔN::EYFP-Fmi complex into the cytoplasm or the distribution of Fmi on the cell surface as nonfunctional complexes. To examine these possibilities, we studied subcellular localization of Fmi in the presence or absence of ΔN::EYFP in S2 cells (Fig. 8J,K). A subpopulation of Fmi molecules were present on the plasma membrane when the Fmi-expressing plasmid was transfected to S2 cells (Fig. 8J). This localization was not dramatically altered in the steady

state when ΔN::EYFP was coexpressed (Fig. 8K). Therefore, this result appears to be consistent with the latter hypothesis of the presence of ΔN::EYFP-Fmi on the cell surface, although it was difficult to rule out the possibility that ΔN::EYFP affected kinetics of both transport and endocytosis of Fmi.

Our above results, obtained by using imaginal epithelia and cultured cells, are consistent with the hypothesis that overexpressed ΔN::EYFP molecules bind endogenous Fmi and form nonfunctional complexes and that, although the complex stays on plasma membrane domains, Fmi is redistributed out of dendro-dendritic interfaces. This relocation of Fmi would consequently hinder Fmi-mediated intercellular communication that should elicit avoidance between dorsal dendritic terminals (Fig. 10B).

Misexpression of ΔN::EYFP leads to effects opposite to that of Fmi on planar polarity

Considering multiple in vivo roles of Fmi, we examined how individual mutant forms would behave in epithelial planar cell polarity (PCP), in which Fmi acts through one of the Fz signaling pathways (PCP pathway). Activity of polarity regulators can be easily assayed by overexpression. One of such gain-of-function phenotypes is generated when protein levels are gradient along the anterior-posterior axis in the wing (Fig. 9A-D) (Adler et al., 1997; Usui et al., 1999). Wing hairs point up the gradient of increasing Fmi levels, whereas they point towards the lower concentration of the Fz gradient (Fig. 9B,D). Misexpression of Fmi::EYFP or ΔC tail caused the pointing-up phenotype, just like when Fmi is overexpressd. By contrast, misexpression of ΔN::EYFP caused the pointing-down phenotype (Fig. 9C), which is opposite to the effect of Fmi overexpression, and strikingly similar to that of Fz overexpression.

Fmi misexpression not only reorients polarity of wing hairs within the expression domain, but also generates non-cell autonomous effects (Tree et al., 2000). These effects can be detected by visualizing the distribution of endogenous Fmi at the cell-boundary and of other components of the PCP pathway, such as Dishevelled (Dsh), that are normally localized at proximal/distal (P/D) boundaries (Fig. 9H, arrow). Under our conditions of ΔN::EYFP overexpression, endogenous Fmi was relocated from P/D boundaries to anterior/posterior (A/P) boundaries, not only within the expression domain but also in a 2-3 cell-wide stripe that juxtaposed overexpressing cells (Fig. 9H, arrowhead and bracket). The non-cell autonomous effect of ΔN::EYFP was also seen as the reorientation of apical structures of adult cuticle cells (Fig. 9I-M). ΔN::EYFP-overexpressing clones (ΔN::EYFP+ clones, stained blue in Fig. 9I-M) caused wing hairs and trichomes of neighboring cells to point away from the clones (Fig. 9J-M). This non-autonomous effect was exactly the opposite of that of Fmi+ clones, but was identical to the phenotype of Fz+ clones (Strutt, 2001; Tree et al., 2002). These opposite effects of polarity between Fmi and ΔN::EYFP expression cannot be explained simply by the fact that ΔN::EYFP decreased endogenous Fmi levels at cell boundaries, because *fmi* loss-of-function clones did not produce an obvious non-cell autonomous effect (Usui et al., 1999). The above effects of ΔN::EYFP overexpression depended on Fz, as shown by the fact that the overexpression phenotype did not appear in *fz* mutants (data not shown). This result supports the possibility that ΔN::EYFP cooperates with Fz to transduce the polarizing signal.

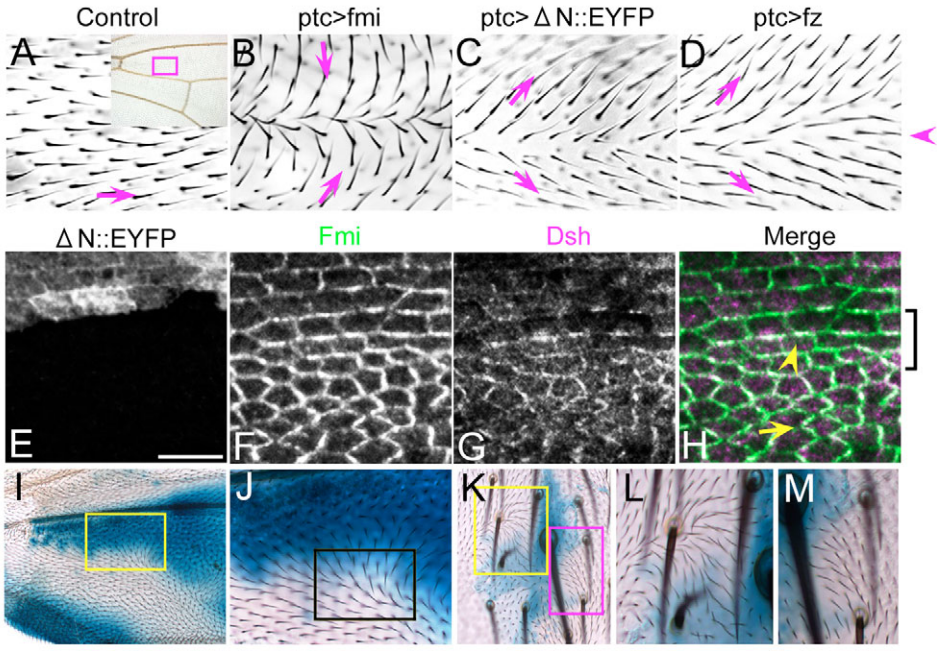

Fig. 9. Effects of Fmi or ΔN::EYFP overexpression on planar cell polarity. (A-M) The effect of ΔN::EYFP expression on planar polarity was addressed in (A-D,I,J) adult wings, (E-H) a pupal wing at 30 hours after puparium formation, and (K-M) an adult notum. Anterior is at the top (A-M), and proximal is to the left (A-J). (A) Control wing. Inset shows higher-magnification image of the boxed area. (B-D) Either (B) full-length Fmi, (C) ΔN::EYFP or (D) Fz were expressed in a region between vein 3 and vein 4 by using *ptc*-Gal4, which drives short-range gradient expression along the anterior-posterior axis of the wing. Arrowhead in D indicates probable peak of the expression level in. Arrows indicate directions of reoriented wing. (E-H) Triple-staining of a ΔN::EYFP-expressing pupal wing for (E) EYFP, (F) endogenous Fmi (see magenta in H) and (G) Dsh (see green in H). A small area that straddled the boundary of the expression domain is shown at high magnification. In contrast to the normal preferential P-D distribution (arrow in H), endogenous Fmi was located substantially at A-P boundaries (arrowhead in H) in the 2-3 cells-wide stripe adjacent to the ΔN::EYFP-producing cells. See text for details. Bar in E: 5 μm for E-H. (I-M) ΔN::EYFP-expressing clones were identified by X-Gal staining. Yellow-boxed areas in I and K are shown magnified in J and L; magenta-boxed area in K is shown enlarged in M. Notice that wing hairs (black box in J) and trichomes (L,M) are pointing away from the clone boundaries. The relevant genotype was *hs-FLP*; *AyGal4 UAS-lacZ/UAS-ΔN::EYFP*.

Journal of Cell Science

Discussion

On the basis of our extensive structure-function analysis, we propose a hypothesis for the molecular functions of Fmi. To control dendritic morphogenesis in the embryo, one likely molecular function of Fmi is that of a receptor for a yet-to-be-identified ligand and that this hypothetical Fmi-ligand interaction is responsible for appropriate pausing of branch elongation (Fig. 10A). This hypothesis also explains an axon-retraction effect by Fmi overexpression in the mushroom body (Reuter et al., 2003). The partial rescue activity of ΔN::EYFP could be due to weak binding to such a hypothetical ligand. ΔN::EYFP retains its HRM domain and, consistently, our structure-function analysis of the mammalian 7-pass transmembrane cadherin Celsr2 also implied a functional role for an extracellular subregion that includes the HRM domain (Shima et al., 2004). These results suggest that the role of this domain to control dendritic growth is conserved among species.

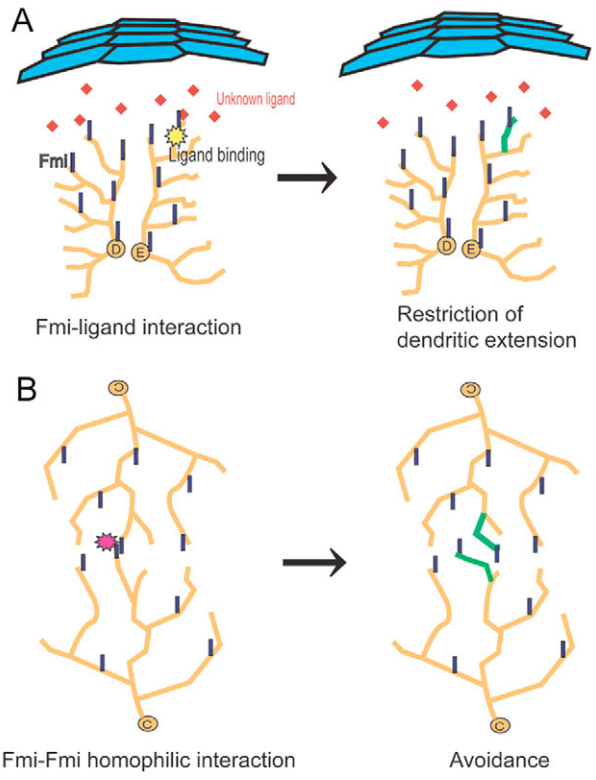

Fig. 10. Models for dual Fmi functions in dendritic morphogenesis. Diagrams show models of putative Fmi function at two distinct phases of dendritic morphogenesis. (A) Branch outgrowth in the embryo. For simplicity, only ddaD and ddaE are illustrated. Fmi (indigo bars) that is expressed in neurons binds to an unknown ligand (red diamonds). Fmi-ligand binding (yellow star) elicits inhibitory signaling against branch extension. A dendritic branch that responded to this signal is indicated as a green bar (right panel). In this illustration, a source of this ligand is hypothesized to be located dorsally in non-neural cells. The secreted ligand is postulated to not propagate very far, but to stay close to its source. (B) Inhibitory communication at dendro-dendritic interfaces in larvae. Class IV da (ddaC) neurons extend dendritic terminals that encounter terminals of contralateral counterparts along the dorsal midline. Signaling occurs at the interfaces, triggerd by Fmi-Fmi homophilic interaction (magenta star). In turn, this triggers local signal transduction of heteroneuronal avoidance (green dendritic branches at the right).

In contrast to rescue activity of ΔN::EYFP towards the embryonic overextension phenotype, ΔN::EYFP is a loss-of-function and dominant-negative form in the inhibitory interaction at dendro-dendritic interfaces in the larval stage. The molecular nature of ΔN::EYFP was investigated in imaginal discs and in cultured cells. Fmi molecules in ΔN::EYFP-expressing cells in the disc were not held back in the ER or Golgi on their way to cell membranes. In addition, coexpression experiments in cultured cells showed that, ΔN::EYFP bound to Fmi and ΔN::EYFP expression did not dramatically alter the distribution of Fmi at the plasma-membrane, which suggests the possibility that ΔN::EYFP-Fmi complexes stay on the cell surface but out of contact sites, where abutting cells express ΔN::EYFP. The simplest explanation of the effect of ΔN::EYFP expression at dendro-dendritic interfaces is that, Fmi-Fmi interaction plays a role in the mutual avoidance during dynamic cycles of terminal extension and retraction, and this interaction is supported by homophilic interaction of cadherin domains (Fig. 10B). In addition to the likely role of this trans Fmi-Fmi homophilic interaction, other possibilities are not excluded. For example, cis or lateral interaction of Fmi might recruit other cell surface receptors and ligands responsible for the bi-directional signaling for avoidance, such as Eph and ephrin.

We interpreted different results of ΔN::EYFP expression in the two distinct rescue experiments such that Fmi exerts two types of molecular interactions. Although we showed that both the full-length form (Fmi::EYFP) and the short form (ΔN::EYFP) were produced at similar levels in da neurons of our transgenic flies, it is difficult to totally rule out the possibility that different processes of dendritogenesis (elongation vs interneuronal avoidance) require different threshold levels of protein activity. Our hypothesis needs to be further tested by investigating functional interactions between Fmi and other molecules that operate in dendritogenesis, and by pursuing other approaches to identify binding partners of Fmi.

Materials and Methods

Molecular cloning

Enhanced yellow fluorescent protein (EYFP, Clontech) was fused to the C-terminal of Fmi by using a spacer, GRVGGGGSGGGGSGGGGSSVD (Huston et al., 1988; Chaudhary et al., 1989). Detailed structures of mutant forms of Fmi and additional information about molecular cloning is available upon request.

Drosophila strains

To express the different forms of Fmi, we used the GAL4-UAS system (Brand and Perrimon, 1993), cloned individual constructs into pUAST and produced transgenic flies as described earlier (Robertson et al., 1988). To visualize dendrites and/or express transgenes, we used the following GAL4 insertions: *IH1*, *IG1-1*, *IG1-2*, *NP1161*, *NP2225*, *NP7028* (Sugimura et al., 2003; Sugimura et al., 2004), *NP1015* (D. Satoh, personal communication), *109(2)80* (Gao et al., 1999), *Gal4 1407* (Luo et al., 1994), *ppk-Gal 4* [which we had generated according to Ainsley et al. (Ainsley et al., 2003)], *patched-Gal4* (Hinz et al., 1994) and *Ay-Gal4* (Ito et al., 1997). *IH1*, *IG1-1*, and *IG1-2* were derived from the collection of Schüpbach and Wieschaus (Schüpbach and Wieschaus, 1998). 'NP' stands for strains that were established by the NP consortium (Hayashi et al., 2002). To express fluorescently labeled proteins, we used *UAS-GFP[S65T]* (Bloomington Stock Center #1521), *UAS-mCD8-GFP* (#5137), and *UAS-Venus-pm* (Sugimura et al., 2003). ΔN::EYFP-expressing clones were made with the Ay-gal4 system (Ito et al., 1997), and a relevant genotype was *hsp-70-flp/+*; *Ay-gal4 UAS-lacZ/UAS-ΔN::EYFP*. Other strains used were *fmi* mutants (fmi^{E45}, fmi^{E59}, and fmi^{72}) (Usui et al., 1999; Gao et al., 2000) and *ppk-EGFP*, a marker for class IV da neurons (Grueber et al., 2003). All embryos and larvae were grown at 25°C.

Journal of Cell Science

Two other extracellular deletions (ΔHR::EYFP and ΔCR:EYFP), which retained much larger extracellular regions than ΔN::EYFP, did not allow the mutant embryos to recover from the phenotype to an extent that could be detected by following our protocol (Fig. 1 and Fig. 2J). Although we found that ΔHR::EYFP and ΔCR:EYFP – when expressed in S2 cells or in salivary glands – were present on plasma membranes (data not shown), both forms appeared to be nonfunctional because they were unable to prevent the overgrowth phenotype. Two other assays are summarized in Fig. 1, the cell aggregation assay (Fig. 8) and an assay to examine an activity in planar cell polarity (PCP). We tested whether or not misexpression of each Fmi form in the wing was able to reorient wing hairs (Fig. 9). In contrast to Fmi, Fmi::EYFP, and ΔC tail, ΔHR::EYFP and ΔCR:EYFP did not exhibit detectable activity in any of these assays. Dendritic distributions and expression levels of ΔHR::EYFP and ΔCR:EYFP were comparable with that of Fmi::EYFP as were those of ΔN::EYFP (see Fig. 2L,M).

Inactivity of ΔHR::EYFP and ΔCR:EYFP was reminiscent of results of in vivo structure-function analysis of *D*E-cadherin (Oda and Tsukita, 1999). In the *D*E-cadherin molecule, the last cadherin repeat is followed by EGF-like domains and a laminin G domain. Internal deletions of these motifs cause a reduction in, or loss of activities of, cell adhesion and rescuing mutants. In Fmi and *D*E-cadherin, such deletions might affect folding of the entire ectodomains. Consequently, it might be that cadherin repeats are misoriented and the mutant molecules no longer retain the homophilic binding property (Oda and Tsukita, 1999).

Within the intracellular C-terminal tail (C tail) of Fmi, a part in the middle includes residues that are conserved among the Fmi family (Shima et al., 2004, see supplementary fig. S1 within). We thus asked how important is the C tail for Fmi function? Expression of the ΔC tail in S2 cells form caused formation of cell aggregate (Fig. 8D) and its expression in wing epidermis was capable of reorienting planar polarity (data not shown). Yet, the ΔC tail did not rescue the dendritic overgrowth (Fig. 2H). This result suggests that the C tail plays an indispensable role in dendrite morphogenesis but that it is not essential to control PCP when misexpressed.

Image collection of dendritic trees

For most experiments, larvae and dechorionized embryos were washed in 0.7% NaCl and 0.3% Triton X-100, placed on glass slides and mounted in PBS. Prior to observation the slides were kept at 4°C for a few hours to arrest movement of the specimens. Because dendrites extend on 2D planes almost underneath the epidermis, *Z*-series of dorsal front images were projected into 2D images, which were then used to measure the distance between dendritic tips and the midline. Time-lapse analysis was done basically as described previously (Sugimura et al., 2003), except that embryos were mounted on dishes with a glass base, and larvae (12 hours after hatching) were mounted in 45% glycerol. Images were collected with a laser scanning confocal microscope LSM510 (Carl Zeiss) and processed with Adobe Photoshop (Adobe Systems). To track entire dendritic branches, we removed signals of gut, epidermis and unknown non-neuronal cells located just above or underneath the branches from individual *Z*-sections before projection (Fig. 5D-F).

Cell ablation

In each experiment, an fmi^{72}/fmi^{E59} embryo 20-22 hours after egg laying (AEL) was manually dechorionated, placed on a coverslip and mounted on a slide between spacers made of tape. Individual da neurons in the dorsal cluster were identified under a fluorescence microscope (Olympus) on the basis of their stereotypic arrangement and the shape of cell body. All neurons, except for the class IV da neurons ddaC, of one hemi-segment were ablated by using Micropoint (Photonics Instruments) as described previously (Sugimura et al., 2004). The coverslip was immediately turned over, the embryo was rotated, and then target cells in the contralateral hemi-segment were ablated. The animal was subsequently imaged at about 40 hours AEL.

Histochemistry

Wing imaginal discs and pupal wings were fixed in 3.7% formaldehyde and 0.05% Triton X-100 in PBS, at room temperature for 1 hour or at 4°C overnight, and stained with the following primary antibodies: mouse or rat anti-Fmi (Usui et al., 1999), rat anti-Dsh (Shimada et al., 2001) or rabbit anti-GFP (Molecular Probes). X-Gal staining was carried out according to Hama et al. (Hama et al., 1990) with a slight modification. Wings were dissected from freshly eclosed flies, submerged in 25% EM-grade glutaraldehyde for 2 minutes, immediately washed with PBS, and incubated in X-Gal solution overnight at 37°C. For the staining of adult notums, muscles and other tissues were removed from the thorax, fixed with 1% EM-grade glutaraldehyde in PBS for a few minutes at room temperature, and then processed as described above.

Cell culture and aggregation assay

Fmi or Fmi mutant forms were transiently expressed in S2 cells by co-transfecting individual pUAST plamsids with *actin5C-Gal4* (a gift from Yash Hiromi) and pUAST-EGFP. Cell aggregation assays were carried out basically as described (Oda et al., 1994). To examine whether ΔN::EYFP was able to inhibit Fmi-dependent aggregation or not, we co-transfected S2 cells with *actin5C-Gal4*, pUAS-EGFP, pUAS-Fmi, and pUAS-ΔN::EYFP or the control pUAST vector at the weight ratio of 1:2:2:20. Spreading of S2 cells on concanavalin A (ConA)-coated dishes was done essentially as described (Rogers et al., 2002).

Immunoprecipitation

Fmi and HA-ΔN::EYFP were transiently expressed in HEK293T cells by using Fugene6 (Roche Diagnostics) according to the manufacturer's instructions. Cell lysis and immunoprecipitation were done as described previously (Iwai et al., 1997). Immunoprecipitation were performed either with anti-myc 9E10 (Santa Cruz), anti-HA 16B12 (BAbCO), or anti-Fmi monoclonal antibody #71, and blotted with another anti-Fmi antibody #74, as described in Usui et al. (Usui et al., 1999).

We thank the Bloomington Stock Center and *Drosophila* Genetic Resource Center in Kyoto Institute of Technology for *Drosophila* stocks; and Akira Nagafuchi and Toshihiko Fujimori for critical discussion and encouragement. This work was supported by the following grants to T. Uemura: CREST from Japan Science and Technology Agency; Grant-in-Aid for Scientific Research on Priority Areas-Molecular Brain Science from the Ministry of Education, Science, Culture, Sports, Science, and Technology of Japan; and Research Grants from Toray Foundation (Japan) for the Promotion of Science and Brain Science Foundation.

References

Adler, P. N. (2002). Planar signaling and morphogenesis in Drosophila. *Dev. Cell* **2**, 525-535.

Adler, P. N., Krasnow, R. E. and Liu, J. (1997). Tissue polarity points from cells that have higher Frizzled levels towards cells that have lower Frizzled levels. *Curr. Biol.* **7**, 940-949.

Ainsley, J. A., Pettus, J. M., Bosenko, D., Gerstein, C. E., Zinkevich, N., Anderson, M. G., Adams, C. M., Welsh, M. J. and Johnson, W. A. (2003). Enhanced locomotion caused by loss of the *Drosophila* DEG/ENaC protein Pickpocket1. *Curr. Biol.* **13**, 1557-1563.

Asmann, Y. W., Dong, M., Ganguli, S., Hadac, E. M. and Miller, L. J. (2000). Structural insights into the amino-terminus of the secretin receptor: I. Status of cysteine and cystine residues. *Mol. Pharmacol.* **58**, 911-919.

Bodmer, R., Barbel, S., Sheperd, S., Jack, J. W., Jan, L. Y. and Jan, Y. N. (1987). Transformation of sensory organs by mutations of the cut locus of *D. melanogaster*. *Cell* **51**, 293-307.

Brand, A. H. and Perrimon, N. (1993). Targeted gene expression as a means of altering cell fates and generating dominant phenotypes. *Development* **118**, 401-415.

Campos-Ortega, J. A. and Hartenstein, V. (1997). *The Embryonic Development of Drosophila melanogaster*. Berlin: Springer.

Chae, J., Kim, M. J., Goo, J. H., Collier, S., Gubb, D., Charlton, J., Adler, P. N. and Park, W. J. (1999). The *Drosophila* tissue polarity gene starry night encodes a member of the protocadherin family. *Development* **126**, 5421-5429.

Chaudhary, V. K., Queen, C., Junghans, R. P., Waldmann, T. A., FitzGerald, D. J. and Pastan, I. (1989). A recombinant immunotoxin consisting of two antibody variable domains fused to Pseudomonas exotoxin. *Nature* **339**, 394-397.

Curtin, J. A., Quint, E., Tsipouri, V., Arkell, R. M., Cattanach, B., Copp, A. J., Henderson, D. J., Spurr, N., Stanier, P., Fisher, E. M. et al. (2003). Mutation of Celsr1 disrupts planar polarity of inner ear hair cells and causes severe neural tube defects in the mouse. *Curr. Biol.* **13**, 1129-1133.

Eaton, S. (2003). Cell biology of planar polarity transmission in the *Drosophila* wing. *Mech. Dev.* **120**, 1257-1264.

Formstone, C. J. and Little, P. F. (2001). The flamingo-related mouse Celsr family (Celsr1-3) genes exhibit distinct patterns of expression during embryonic development. *Mech. Dev.* **109**, 91-94.

Formstone, C. J. and Mason, I. (2005). Combinatorial activity of Flamingo proteins directs convergence and extension within the early zebrafish embryo via the planar cell polarity pathway. *Dev. Biol.* **282**, 320-335.

Fujimori, T. and Takeichi, M. (1993). Disruption of epithelial cell-cell adhesion by exogenous expression of a mutated nonfunctional N-cadherin. *Mol. Biol. Cell* **4**, 37-47.

Gao, F. B., Brenman, J. E., Jan, L. Y. and Jan, Y. N. (1999). Genes regulating dendritic outgrowth, branching, and routing in Drosophila. *Genes Dev.* **13**, 2549-2561.

Gao, F. B., Kohwi, M., Brenman, J. E., Jan, L. Y. and Jan, Y. N. (2000). Control of dendritic field formation in Drosophila: the roles of flamingo and competition between homologous neurons. *Neuron* **28**, 91-101.

Grueber, W. B., Jan, L. Y. and Jan, Y. N. (2002). Tiling of the *Drosophila* epidermis by multidendritic sensory neurons. *Development* **129**, 2867-2878.

Grueber, W. B., Ye, B., Moore, A. W., Jan, L. Y. and Jan, Y. N. (2003). Dendrites of distinct classes of *Drosophila* sensory neurons show different capacities for homotypic repulsion. *Curr. Biol.* **13**, 618-626.

Hama, C., Ali, Z. and Kornberg, T. B. (1990). Region-specific recombination and expression are directed by portions of the *Drosophila* engrailed promoter. *Genes Dev.* **4**, 1079-1093.

Hayashi, S., Ito, K., Sado, Y., Taniguchi, M., Akimoto, A., Takeuchi, H., Aigaki, T.,

Matsuzaki, F., Nakagoshi, H., Tanimura, T. et al. (2002). GETDB, a database compiling expression patterns and molecular locations of a collection of Gal4 enhancer traps. *Genesis* **34**, 58-61.
Hinz, U., Giebel, B. and Campos-Ortega, J. A. (1994). The basic-helix-loop-helix domain of *Drosophila* lethal of scute protein is sufficient for proneural function and activates neurogenic genes. *Cell* **76**, 77-87.
Hirano, S., Suzuki, S. T. and Redies, C. (2003). The cadherin superfamily in neural development: diversity, function and interaction with other molecules. *Front. Biosci.* **8**, D306-D355.
Huston, J. S., Levinson, D., Mudgett-Hunter, M., Tai, M. S., Novotny, J., Margolies, M. N., Ridge, R. J., Bruccoleri, R. E., Haber, E., Crea, R. et al. (1988). Protein engineering of antibody binding sites: recovery of specific activity in an anti-digoxin single-chain Fv analogue produced in Escherichia coli. *Proc. Natl. Acad. Sci. USA* **85**, 5879-5883.
Ito, K., Awano, W., Suzuki, K., Hiromi, Y. and Yamamoto, D. (1997). The *Drosophila* mushroom body is a quadruple structure of clonal units each of which contains a virtually identical set of neurones and glial cells. *Development* **124**, 761-771.
Iwai, Y., Usui, T., Hirano, S., Steward, R., Takeichi, M. and Uemura, T. (1997). Axon patterning requires DN-cadherin, a novel neuronal adhesion receptor, in the *Drosophila* embryonic CNS. *Neuron* **19**, 77-89.
Jan, Y. N. and Jan, L. Y. (2003). The control of dendrite development. *Neuron* **40**, 229-242.
Lee, R. C., Clandinin, T. R., Lee, C. H., Chen, P. L., Meinertzhagen, I. A. and Zipursky, S. L. (2003). The protocadherin Flamingo is required for axon target selection in the *Drosophila* visual system. *Nat. Neurosci.* **6**, 557-563.
Luo, L., Liao, Y. J., Jan, L. Y. and Jan, Y. N. (1994). Distinct morphogenetic functions of similar small GTPases: *Drosophila* Drac1 is involved in axonal outgrowth and myoblast fusion. *Genes Dev.* **8**, 1787-1802.
Mlodzik, M. (2002). Planar cell polarization: do the same mechanisms regulate *Drosophila* tissue polarity and vertebrate gastrulation? *Trends Genet.* **18**, 564-571.
Oda, H. and Tsukita, S. (1999). Nonchordate classic cadherins have a structurally and functionally unique domain that is absent from chordate classic cadherins. *Dev. Biol.* **216**, 406-422.
Oda, H., Uemura, T., Harada, Y., Iwai, Y. and Takeichi, M. (1994). A *Drosophila* homolog of cadherin associated with armadillo and essential for embryonic cell-cell adhesion. *Dev. Biol.* **165**, 716-726.
Ozawa, M. (2002). Lateral dimerization of the E-cadherin extracellular domain is necessary but not sufficient for adhesive activity. *J. Biol. Chem.* **277**, 19600-19608.
Patel, S. D., Chen, C. P., Bahna, F., Honig, B. and Shapiro, L. (2003). Cadherin-mediated cell-cell adhesion: sticking together as a family. *Curr. Opin. Struct. Biol.* **13**, 690-698.
Reuter, J. E., Nardine, T. M., Penton, A., Billuart, P., Scott, E. K., Usui, T., Uemura, T. and Luo, L. (2003). A mosaic genetic screen for genes necessary for *Drosophila* mushroom body neuronal morphogenesis. *Development* **130**, 1203-1213.
Robertson, H. M., Preston, C. R., Phillis, R. W., Johnson-Schlitz, D. M., Benz, W. K. and Engels, W. R. (1988). A stable genomic source of P element transposase in *Drosophila melanogaster*. *Genetics* **118**, 461-470.
Rogers, S. L., Rogers, G. C., Sharp, D. J. and Vale, R. D. (2002). *Drosophila* EB1 is important for proper assembly, dynamics, and positioning of the mitotic spindle. *J. Cell Biol.* **158**, 873-884.
Schupbach, T. and Wieschaus, E. (1998). Probing for gene specificity in epithelial development. *Int. J. Dev. Biol.* **42**, 249-255.
Senti, K. A., Usui, T., Boucke, K., Greber, U., Uemura, T. and Dickson, B. J. (2003). Flamingo regulates r8 axon-axon and axon-target interactions in the *Drosophila* visual system. *Curr. Biol.* **13**, 828-832.
Shima, Y., Copeland, N. G., Gilbert, D. J., Jenkins, N. A., Chisaka, O., Takeichi, M. and Uemura, T. (2002). Differential expression of the seven-pass transmembrane cadherin genes Celsr1-3 and distribution of the Celsr2 protein during mouse development. *Dev. Dyn.* **223**, 321-332.
Shima, Y., Kengaku, M., Hirano, T., Takeichi, M. and Uemura, T. (2004). Regulation of dendritic maintenance and growth by a mammalian 7-pass transmembrane cadherin. *Dev. Cell* **7**, 205-216.
Shimada, Y., Usui, T., Yanagawa, S., Takeichi, M. and Uemura, T. (2001). Asymmetric colocalization of Flamingo, a seven-pass transmembrane cadherin, and Dishevelled in planar cell polarization. *Curr. Biol.* **11**, 859-863.
Strutt, D. I. (2001). Asymmetric localization of frizzled and the establishment of cell polarity in the *Drosophila* wing. *Mol. Cell* **7**, 367-375.
Strutt, D. (2003). Frizzled signalling and cell polarisation in *Drosophila* and vertebrates. *Development* **130**, 4501-4513.
Sugimura, K., Yamamoto, M., Niwa, R., Satoh, D., Goto, S., Taniguchi, M., Hayashi, S. and Uemura, T. (2003). Distinct developmental modes and lesion-induced reactions of dendrites of two classes of *Drosophila* sensory neurons. *J. Neurosci.* **23**, 3752-3760.
Sugimura, K., Satoh, D., Estes, P., Crews, S. and Uemura, T. (2004). Development of morphological diversity of dendrites in *Drosophila* by the BTB-zinc finger protein abrupt. *Neuron* **43**, 809-822.
Sweeney, N. T., Li, W. and Gao, F. B. (2002). Genetic manipulation of single neurons in vivo reveals specific roles of flamingo in neuronal morphogenesis. *Dev. Biol.* **247**, 76-88.
Tepass, U., Truong, K., Godt, D., Ikura, M. and Peifer, M. (2000). Cadherins in embryonic and neural morphogenesis. *Nat. Rev. Mol. Cell. Biol.* **1**, 91-100.
Tissir, F., De-Backer, O., Goffinet, A. M. and Lambert de Rouvroit, C. (2002). Developmental expression profiles of Celsr (Flamingo) genes in the mouse. *Mech. Dev.* **112**, 157-160.
Tissir, F., Bar, I., Jossin, Y. and Goffinet, A. M. (2005). Protocadherin Celsr3 is crucial in axonal tract development. *Nat. Neurosci.* **8**, 451-457.
Tree, D. R., Shulman, J. M., Rousset, R., Scott, M. P., Gubb, D. and Axelrod, J. D. (2002). Prickle mediates feedback amplification to generate asymmetric planar cell polarity signaling. *Cell* **109**, 371-381.
Uemura, T. and Shimada, Y. (2003). Breaking cellular symmetry along planar axes in drosophila and vertebrates. *J. Biochem. (Tokyo)* **134**, 625-630.
Usui, T., Shima, Y., Shimada, Y., Hirano, S., Burgess, R. W., Schwarz, T. L., Takeichi, M. and Uemura, T. (1999). Flamingo, a seven-pass transmembrane cadherin, regulates planar cell polarity under the control of Frizzled. *Cell* **98**, 585-595.
Veeman, M. T., Axelrod, J. D. and Moon, R. T. (2003). A second canon. Functions and mechanisms of beta-catenin-independent Wnt signaling. *Dev. Cell* **5**, 367-377.
Yagi, T. and Takeichi, M. (2000). Cadherin superfamily genes: functions, genomic organization, and neurologic diversity. *Genes Dev.* **14**, 1169-1180.
Ye, B. and Jan, Y. N. (2005). The cadherin superfamily and dendrite development. *Trends Cell Biol.* **15**, 64-67.

Journal of Cell Science